 doi:10.20944/preprints202101.0434.v1

Type of the Paper (Article)

Formation of nickel(II)porphyrin and its interaction with DNA in aqueous medium

Ahsan Habib[1*], Salma Serniabad[1,2], Mohammad Shamim Khan[1], Rokayea Islam[1], Mrittika Chakraborty[1], Aklima Nargis[1], Md Emran Quayum[1], Md Ashraful Alam[2], Valentina Rapozzi[3], Masaaki Tabata[4]

[1] Department of Chemistry, University of Dhaka, Faculty of Science, Dhaka-1000, Bangladesh; habib-chem@du.ac.bd
[2] Department of Applied Chemistry and Chemical Engineering, Noakhali Science and Technology University, Noakhali 3814, Bangladesh
[3] Department of Medicine, Udine University, P.le Kolbe 4, 33100, Udine, Italy
[4] Department of Chemistry, Faculty of Science and Engineering, Saga University 1, Honjo-machi, Saga 840-8502, Japan
* Correspondence: habibchem@du.ac.bd; Tel.: +8801779227863

Abstract: In this work, kinetics of the reaction between 5,10,15,20-tetrakis(N-methylpyridium-4-yl)porphyrin and Ni^{2+} species were investigated in aqueous solution at 25 ±1 ºC in I = 0.10 M ($NaNO_3$). Speciation of Ni^{2+} was carried out in I = 0.10 M ($NaNO_3$) in order to provide the distribution of the Ni^{2+} species with different solution pH. The experimental data have been compared with the speciation diagram constructed from the values of hydrolysis constants of Ni^{2+} ion. Speciation data showed that the hexaaquanickel(II), $[Ni(H_2O)_6]^{2+}$, ions take place in hydrolysis reactions through formation of $[Ni(OH_2)_{6-n}(OH)_n]^{2-n}$ species with solution pH. Based on the speciation of Ni^{2+} and pH dependent rate constants, rate expression can be written as: $d[Ni(TMPyP)^{4+}]/dt = (k_1[Ni^{2+}_{(aq)}] + k_2[Ni(OH)^{+}_{(aq)}] + k_3[Ni(OH)_2{}^{o}_{(aq)}] + k_4[Ni(OH)_3{}^{-}_{(aq)}])[H_2TMPyP^{4+}]$, where k_1, k_2, k_3 and k_4 were found to be $k_1 = (0.62 \pm 0.22) \times 10^{-2}$; $k_2 = (3.60 \pm 0.40) \times 10^{-2}$; $k_3 = (2.09 \pm 0.52) \times 10^{-2}$, $k_4 = (0.53 \pm 0.04) \times 10^{-2}$ $M^{-1}s^{-1}$ at 25 ±1 °C, respectively. Kinetic results showed that monohydroxo, $[Ni(H_2O)_5(OH)]^{+}$, is the most reactive among the $[Ni(OH_2)_{6-n}(OH)_n]^{2-n}$ species. The enhanced reactivity has been ascribed to the formation of hydrogen bonding between oxygen atom of hydroxyl group of the $[Ni(H_2O)_5(OH)]^{+}$ species and the pyrrolic hydrogen atom of the $[H_2TMPyP]^{4+}$. The rate of formation of $[Ni(II)TMPyP]^{4+}$ complex was to be 3.99×10^{-2} $M^{-1}s^{-1}$ in I = 0.10 M, $NaNO_3$ (25 ± 1 ºC). Ionic strength effect on the reaction rate is suggested that the net charge of the tetracationic porphyrin is to be +3.6 on the basis of Brønsted-Bjerrum equation. The UV-Vis and fluorescence data revealed that $[Ni(II)TMPyP]^{4+}$ and $H_2(TMPyP)^{4+}$ interact with DNA, and UV-Vis results suggest that Ni(II)-porphyrin and free base porphyrin interact with DNA via outside binding with self-stacking and intercalation, respectively. Mechanism of kinetics of formation of the $[Ni(II)TMPyP]^{4+}$ complex in aqueous medium is discussed. An investigation of application of the $[Ni(II)TMPyP]^{4+}$ complex along with other metalloporphyrins such as Zn^{2+}-, Ru^{2+}-, Pt^{2+}-, $[Au(III)TMPyP]^{5+}$ as anti-COVID-19 agents is now in progress under international collaboration.

Keywords: Speciation of Ni^{2+}; Kinetics and mechanism; Hydrogen bonding; 5,10,15,20-tetrakis(N-methylpyridium-4-yl)porphyrinatonickel(II) tetracation; Outside binding; Chemotherapeutic agents.

1. Introduction

Substantial studies by many research groups have been carried out on kinetics and mechanism of formation of metalloporphyrins because of their possible applications as therapeutic agents in medical as well as in biological fields [1-16]. Moreover, the structural similarity of the porphyrins with chlorophylls, green pigments of leaves, has been attracted by the researchers for their potential use in artificial photosynthetic system [17].

Preprints (www.preprints.org) | NOT PEER-REVIEWED | Posted: 22 January 2021 doi:10.20944/preprints202101.0434.v1

In the human body system, the protoporphyrin IX ring is continuously synthesized during biosynthesis of heme, and iron(II) is subsequently coordinated to the porphyrin core. Studies of kinetics of incorporation of metal ions into the porphyrins' core give the mechanistic pathways of the formation of metalloporphyrins. By knowing proper reaction pathways of formation of metalloporphyrins, it may possible to formulate porphyrin-based new drugs. Hambright and Chock (1974) proposed a general mechanism of formation of metalloporphyrins for the first time, and later that was reviewed by a number of research groups [18-25]. Open chain-ligands exhibit significant reactivity in formation of metallocomplexes while macrocyclic ligands, for example, porphyrins, show poor reactivity because of their complex nature [26]. Several approaches have already been executed to accelerate the metalation reaction of the porphyrins. Some of the events should be approaches: (i) substitution reactions of cadmium(II) or mercury(II)porphyrins [27-29], (ii) porphyrins with substituents at the pyrrole nitrogen [30,31], (iii) functionalization of porphyrins (e.g., tetracarboxylic acid "pocket-fence" porphyrins) (iv) performing reactions at a suitable solution pH in presence of metal ions having hydroxo-ligands [20,24,25]. The rate of formation of metalloporphyrins could be enhanced via any of the above-mentioned approaches. Accordingly, a group of researchers showed the enhanced reactivity of macrocyclic porphyrins for the metal ions having hydroxo-ligands [Tanaka, 1983; Habib et al., 2004; Habib et al., 2020]. They reported that the presence of hydroxo-ligands of the metal ions facilitates the formation of hydrogen bonding with the pyrrolic hydrogen atom of the free base porphyrin [20,24,25]. Batinić-Haberle et al. (1999) also studied the metalation reactions of incorporation of Fe^{3+} and Mn^{3+} into the 5,10,15,20-tetrakis(N-alkylpyridiniumyl)porphyrins and they found the enhanced reactivity for the exchange metalation of monohydroxoiron with the aqua-manganese porphyrins because of trans-axial effect [4].

Nickel is an essential element for humans as well as for other animals in functioning many metabolic reactions. The known multifunctional properties of the porphyrinson o and metalloporphyrins have been extended the porphyrins' research in various fields. So, the study of kinetics and mechanism of the formation of Ni(II)porphyrin may open a new research arena of applications of nickel-porphyrin complexes. Reduced form of the nickel-porphyrin complexes acts as enzymatic cofactors (F430) in the global carbon cycle and also used in solar-fuel cells as a powerful catalyst to evolve the hydrogen gas. The reduced nickel-porphyrins have been used in the reduction of CO and CO_2 as well. Nickel is a transition metal having d^8 electronic configuration, thus exhibits least reactivity in complex formation. However, in our previous study, we found enhanced reactivity of Au^{3+} ion in the formation of complexes with the macrocyclic tetrakis(N-methylpyridinium-4-yl)porphyrin, $[H_2TMPyP]^{4+}$, where Au^{3+} ion belongs to the d^8 electronic configuration [24]. According to the speciation diagram of Au^{3+} ion with solution pH, the monohydroxotrichloroaurate(III), $[AuCl_3(OH)]^-$, was found as a predominant species under the experimental condition [4]. The negatively charged $[AuCl_3(OH)]^-$ ion can easily approach the core of the tetracationic porphyrin and the presence of the hydroxo-ligand in the Au^{3+} species causes enhanced reactivity in the formation of the $[Au(III)TMPyP]^{5+}$ complex. This is because the hydroxo-ligand of the $[AuCl_3(OH)]^-$ species forms hydrogen bonding with the pyrrolic hydrogen atom of the porphyrin, which resulted in enhanced rate of the reaction. A number of research groups has also attempted to investigate the kinetics of formation of Ni(II)porphyrins to understand the mechanism of reaction [32-35]. Tan et al. (2011) and Tian et al. (2012) studied the speciation of nickel from the geo- and hydrothermal points of view, however, limited information is available to understand the kinetics of the reaction of Ni^{2+} with H_2TMPyP^{4+} [36,37].

Much attention has been paid to explore the interaction between the cationic porphyrins and nucleic acids, such as DNA and RNA because of promising properties of the porphyrins in medical as well as in biological applications [2,3,5-7,9-16,39-45]. The potential uses of the porphyrins in medical and biological fields are due to their anticancer

Preprints (www.preprints.org) | NOT PEER-REVIEWED | Posted: 22 January 2021 doi:10.20944/preprints202101.0434.v1

[11,12,16], antiviral and/or antibacterial/anti-inflammatory [4,6,10,13-15] and antifungal [6,46] activities. Porphyrins also have potential as imaging agents in the medical imaging systems [6,47-49]. Cationic porphyrins interact with DNA in various modes where substituents of the porphyrins and/or central metal ions play vital roles. The three major modes of interaction between porphyrins and DNA are intercalation, outside binding without self-stacking, and outside binding with self-stacking along the DNA surface [38-41,50,51]. Partial intercalation has also been suggested [40]. It is noteworthy to mention that potential applications of the porphyrins in medical and biological systems depend mainly on the modes of interaction of the porphyrin-DNA adducts. The exploration of NiTE-2-PyP^{4+} as an SOD mimic is worth mentioning [8].

Very recently Liu and Li (2020) studied the severe health effect by the novel coronavirus (COVID-19) worldwide by applying theoretical models [52]. They used conserved domain analysis, homology modeling and molecular docking models to compare the biological roles of specific proteins of the COVID-19, and found the novel coronavirus attacks the 1-beta chain of the hemoglobin and captures the protoporphyrin IX to inhibit human heme metabolism. The theoretical results suggest that the COVID-19 has strong affinity for the porphyrins and/or metalloporphyrins. The noble but clinically relevant finding encouraged us for investigation of possible applications of the porphyrins as anti-COVID-19 agents.

In this paper, speciation of Ni^{2+} in aqueous medium with different solution pH in I = 0.10 M ($NaNO_3$) and 0.10 M NaCl at 25 ±1 °C has been characterized. By applying the distribution of the Ni^{2+} species with solution pH, the kinetics of the formation of [Ni(II)TMPyP]$^{4+}$ complex, I (Scheme 1) has been studied in order to explore the reactions mechanism for the metalation reaction. We have extended our studies on interaction of DNA with the [Ni(II)TMPyP]$^{4+}$ complex along the H_2TMPyP^{4+} in order to investigate their potential applications in the medical as well as in the biological fields. An investigation of the application of porphyrins, particularly Ni^{2+}-, Zn^{2+}-, Ru^{2+}-, Pt^{2+}-, [Au(III)TMPyP]$^{5+}$ as anti-COVID-19 agents is now in progress under international research collaboration.

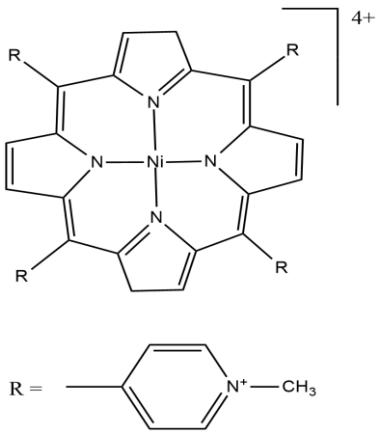

I

Scheme 1. Tetracationic nickel(II)porphyrin, I.

2. Results and discussion

3.1 Speciation of Ni^{2+}

Speciation of Ni^{2+} ion in aqueous solution in the presence of 0.10 M of $NaNO_3$ (I) at 25 ±1 °C was carried out to investigate the kinetics of the reaction between the free base porphyrin, [H_2TMPyP]$^{4+}$, and the Ni^{2+} species. In order to investigate the kinetics of the metalation reaction, it is highly expected to know the speciation of the relevant metal ion. This is because the speciation diagram provides species distribution that is required to establish the reaction mechanism for the relevant reaction. Figure 1 shows the speciation

Preprints (www.preprints.org) | NOT PEER-REVIEWED | Posted: 22 January 2021 doi:10.20944/preprints202101.0434.v1

diagram generated from the hydrolysis constants of Ni^{2+} species with the solution pH [53]. As seen from Fig. 1, the hexaaqua Ni^{2+}, $[Ni(H_2O)_6]^{2+}$ simply written as $Ni^{2+}_{(aq)}$, species predominantly exists from the acidic to even alkaline pH (~9.50) and is converting to hydroxo species, $[Ni(H_2O)_{6-n}(OH)_n]^{2-n}$, through successive replacement of the H_2O molecule by the OH^- groups with increasing the solution pH. The aqua-monohydroxo Ni2+, $[Ni(H_2O)_5(OH)]^+$, species is distributed from pH ~7.90 to 11.00 with the maximum distribution that observed at pH 9.50 (Fig. 1). Like $Ni^{2+}_{(aq)}$ ions, the monohydroxo Ni^{2+} ions, $[Ni(H_2O)_5(OH)]^+$, are also aquatic species, thus they take part in metalation reaction with the water soluble free base porphyrin, $[H_2TMPyP]^{4+}$, significantly in the aqueous medium.

On the other hand, a small fraction of the dihydroxo Ni^{2+}, $[Ni(H_2O)_4(OH)_2]^0$, species reacts with the free base porphyrin, $[H_2TMPyP]^{4+}$, because of its very poor existence in the aqueous system under the present experimental conditions. The solubility product for the dihydroxo Ni^{2+} species is only K^b_{S10} = -15.7, thus it starts to precipitate at pH ~8.15 for 10-3 M of Ni^{2+} solution [53]. This causes the presence of a small fraction of the $[Ni(H_2O)_4(OH)_2]^0$ species in this study (Fig. 1). According to the speciation diagram, the $[Ni(H_2O)_4(OH)_2]^0$ species is distributed from pH ~8.25 to the higher pH (≥ 12.00) where its maximum distribution is observed at pH ~10.30 (Fig. 1). It is expected that the reactivity for the dihydroxo Ni^{2+}, $[Ni(H_2O)_4(OH)_2]^0$, species towards the free base porphyrin, $[H_2TMPyP]^{4+}$, would be higher than that of the monohydroxo, $[Ni(H_2O)_5(OH)]^+$, species. This is because the dihydroxo species is electrically neutral, thus the $[Ni(H_2O)_4(OH)_2]^0$ species can easily approach to the tetracationic porphyrin's core without any Coulombic force of repulsion while the unipositive aqua monohydroxo Ni^{2+}, $[Ni(H_2O)_5(OH)]^+$, species could suffer from repulsive force. The dihydroxo Ni^{2+} species exists with a small fraction in the aqueous systems because of its very low solubility product, K^b_{S10} = -15.7, under the present experimental conditions ($[Ni^{2+}] = 10^{-3}$ M; I = 0.10 M, $NaNO_3$), therefore, it is reasonable to observe the less reactivity for the $[Ni(H_2O)_4(OH)_2]^0$ species towards the $[H_2TMPyP]^{4+}$ as described in the kinetics section. The trihydroxo Ni^{2+}, $[Ni(H_2O)_3(OH)_3]^-$ species is distributed from pH 9.4 to the higher pH > 12.00 while its distribution is so small ~1-2% at the experimental solution pH, 9.50 (Fig. 1).

The UV-Vis spectral data also confirm the stepwise formation of the hydroxo Ni^{2+}, $[Ni(H_2O)_{6-n}(OH)_n]^{2-n}$, species as a function of the solution pH (supplementary Figure S-1). As mentioned above, the Ni^{2+} exists in aqueous system as hexaaqua, $[Ni(H_2O)_6]^{2+}$, species. The $[Ni(H_2O)_6]^{2+}$ species shows the ligand to metal charge transfer (LMCT) transition and the absorption maximum is centered at λ_{max} = 391 nm in the UV region (supplementary Figure S-1). The LMCT transitions have been assigned due to the charge transfer from bonding or nonbonding p-orbital of ligand to high energy antibonding dp*-orbital of the metal ion [54]. The UV-Vis absorption spectra for Ni^{2+} (1.0×10^{-3} M) in 0.10 M $NaNO_3$ solutions with different solution pH are shown in the supplementary Figure S-1. As seen from supplementary Figure S-1, the intensity of the peak centered at λ_{max} 391 nm that gradually decreases as a function of solution pH and reaches at flat with the higher pH value, ~10.30. This result suggests that the hexaaqua Ni^{2+}, $[Ni(H_2O)_6]^{2+}$, species are converting to hydroxo, $[Ni(H_2O)_{6-n}(OH)_n]^{2-n}$, species through stepwise replacement of the H_2O by the OH^- with increasing the solution pH from 2.97 to 11.40. It is noted that the solution does not show any clear absorption maxima between 350 and 450 nm at pH ≥ 10.30. This is because of formation of the dihydroxo Ni^{2+}, $[Ni(H_2O)_4(OH)_2]^0$, species and then phases out from the aqueous solution as $Ni(OH)_2^0$ (K^b_{S10} = -15.7), thereby resulting in presence of insignificant amount of the UV-active species in the aqueous system (supplementary Figure S-1) [53]. Therefore, it may conclude that the hexaaqua Ni^{2+}, $[Ni(H_2O)_6]^{2+}$, species co-exists with the $[Ni(H_2O)_{6-n}(OH)n]_{2-n}$ [n = 1, ….,6] within a pH range from ~2 to 14 according to the following equations [53]:

Preprints (www.preprints.org) | NOT PEER-REVIEWED | Posted: 22 January 2021 doi:10.20944/preprints202101.0434.v1

$$Ni^{2+}_{(aq)} + OH^- \rightleftharpoons Ni(OH)^+_{(aq)} \quad (1)$$

$$Ni(OH)^+_{aq} + OH^- \rightleftharpoons Ni(OH)_{2(aq)} \quad (2)$$

$$Ni(OH)_{2(aq)} + OH^- \rightleftharpoons Ni(OH)^-_3 \quad (3)$$

$$Ni(OH)^-_3 + OH^- \rightleftharpoons Ni(OH)^{2-}_4 \quad (4)$$

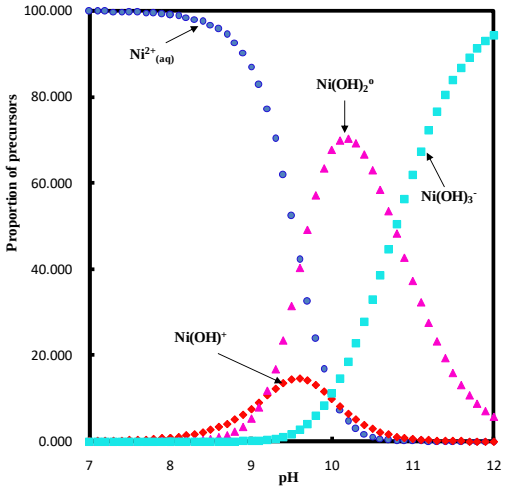

Figure 1. Speciation diagram of Ni^{2+} species as a function of solution pH. The diagram is reproduced on the basis of hydrolysis constants of Ni^{2+} [53].

3.2 Kinetics of formation of $[Ni(II)TMPyP]^{4+}$ complex

Changing the absorbance of the free base porphyrin, $[H_2TMPyP]^{4+}$, at λ_{max} = 422 nm with time is a signature to monitor the progress of formation of the $[Ni(II)TMPyP]^{4+}$ complex. Thus, this event has been taken into account to investigate the kinetics of Ni2+ into the free base porphyrin, $[H_2TMPyP]^{4+}$, in aqueous medium at 25 ±1 °C in I = 0.10 M ($NaNO_3$). The spectral pattern of the formation of the $[Ni(II)TMPyP]^{4+}$ complex is shown in Fig. 7. The variation of the absorbance depicted as $\ln(A_t\text{-}A_\alpha)$ was plotted with time in order to achieve the observed rate constants for the reactions between the $[H_2TMPyP]^{4+}$ and $[Ni(H_2O)_{6\text{-}n}(OH)_n]^{2\text{-}n}$ species as a function of solution pH.

The rate of formation of the $[Ni(II)TMPyP]^{4+}$ complex is first order with respect to the free base porphyrin that can be written by the following equation:

$$-d[H_2TMPyP^{4+}]/dt = k_{obs}[H_2TMPyP^{4+}] = k_f[Ni^{2+}][H_2TMPyP^{4+}] \quad (5)$$

where k_{obs} is the observed first-order rate constant and k_f is the second order formation rate constant.

From the reactions between the $[H_2TMPyP]^{4+}$ and Ni^{2+} species at different solution pH, the observed rate constants (k_{obs}) were measured to explore the reactivity of the various $[Ni(H_2O)_{6\text{-}n}(OH)_n]^{2\text{-}n}$ species. The values of the observed rate constants for the reactions of the free base porphyrins with the Ni^{2+} species as a function of solution pH are shown in Fig. 2. As seen from Figure 2, the observed rate constant increases as a function of the solution pH and goes to its maximum value at pH 9.50 and then slow down as pH is being increased. The rising trend for the rate constants almost remains constant until pH 6.60 and then increases sharply with pH. These results suggest that the reacting species of the Ni^{2+} ion is mostly hexaaqua Ni^{2+} ion, $[Ni(H_2O)_6]^{2+}$ written as $Ni^{2+}_{(aq)}$, within the pH range from 2.97 to ~8.00 which is one of the less reactive among the $[Ni(H_2O)_{6\text{-}n}(OH)_n]^{2\text{-}n}$ [n = 1, ….,6] species (Fig. 1).

Preprints (www.preprints.org) | NOT PEER-REVIEWED | Posted: 22 January 2021 doi:10.20944/preprints202101.0434.v1

Thus, at low pH (3.00 - 6.60) and 0.10 M $NaNO_3$, the main Ni^{2+} species is hexaaqua, $[Ni(H_2O)_6]^{2+}$, and changes to monohydroxo $[Ni(H_2O)_5(OH)^+]$, dihydroxo $[Ni(H_2O)_2(OH)_2^0]$, trihydroxo $[Ni(H_2O)_3(OH)_3^-]$ and tetrahydroxo $[Ni(H_2O)_2(OH)_4^{2-}]$ species as a function of solution pH that stated in equations 1-4. In our previous study, it has also been reported that Zn^{2+} ion exists predominantly as a hexaaqua, $[Zn(H_2O)_6]^{2+}$, species at low pH (~2-5) in 0.10 M $NaNO_3$, and changes to hydroxo species stepwise and finally converts to tetrahydroxo $[Zn(OH)_4^{2-}]$ species at higher solution pH [25].

As mentioned above, Ni^{2+} ion predominantly exists as hexaaquanickel(II), $[Ni(H_2O)_6]^{2+}$, species at solution pH 3.0-8.0 and showed less reactivity in incorporation into the free base porphyrin, H_2TMPyP^{4+}. As the distribution of aqua-monohydroxo, $[Ni(H_2O)_5(OH)]^+$, species increases, the reactivity of the Ni^{2+} ion also increases. As shown in Figure 2, the maximum observed rate constant is found at pH 9.50. This result is confirming the maximum distribution of the $[Ni(H_2O)_5(OH)]^+$ species at pH ~9.50 and thus exhibited the highest reactivity towards the free base porphyrin, $[H_2TMPyP]^{4+}$. With increasing the solution pH, distribution of the aqua-dihydroxo species of Ni^{2+}, $[Ni(H_2O)_4(OH)_2]^0$, is being increased. With further increase the solution pH, the presence of aqua-trihydroxonickelate(II), $[Ni(H_2O)_3(OH)_3]^-$, species is also increased and thus Ni^{2+} becomes less reactive towards the free base porphyrin, $[H_2TMPyP]^{4+}$. Aqua-tetrahydroxonickelate(II), $[Ni(H_2O)_2(OH)_4]^{2-}$, species will be eventually the predominant species at the higher solution pH (~12.00).

Therefore, the rate of incorporation of Ni^{2+} species into the $[H_2TMPyP]^{4+}$ (written H_2P^{4+} is the simplest form of the $[H_2TMPyP]^{4+}$) is expressed by the following equations:

$$Ni^{2+}_{(aq)} + H_2P^{4+} \underset{}{\overset{+\,OH^-}{\rightleftharpoons}} NiP^{4+} + 2H^+ \quad (6)$$

$$Ni(OH)^+_{aq} + H_2P^{4+} \underset{}{\overset{+\,OH^-}{\rightleftharpoons}} NiP^{4+} + H_2O + H^+ \quad (7)$$

$$Ni(OH)_{2(aq)} + H_2P^{4+} \underset{}{\overset{+\,OH^-}{\rightleftharpoons}} NiP^{4+} + 2H_2O \quad (8)$$

$$Ni(OH)^-_{3(aq)} + H_2P^{4+} \underset{}{\overset{+\,OH^-}{\rightleftharpoons}} NiP^{4+} + 2H_2O + OH^+ \quad (9)$$

$$Ni(OH)_4^{2-}{}_{(aq)} + H_2P^{4+} \underset{}{\overset{+\,OH^-}{\rightleftharpoons}} NiP^{4+} + 2H_2O + 2OH^- \quad (10)$$

is in ce the reactivity of the aqua-tetrahydroxonickelate(II), $[Ni(H_2O)_2(OH)_4]^{2-}$, species towards the $[H_2TMPyP]^{4+}$ is very poor and its negligible presence at pH 9.50, thus, equ (10) can be ignored. Therefore, equs (6) to (9) are taken into account in order to calculate the observed rate constants, k_{obs}.

Therefore, $k_{obs} = k_1[Ni^{2+}{}_{(aq)}] + k_2[Ni(OH)^+{}_{(aq)}] + k_3[Ni(OH)_2{}^0{}_{(aq)}] + k_4[Ni(OH)_3{}^-{}_{(aq)}]$ (11)

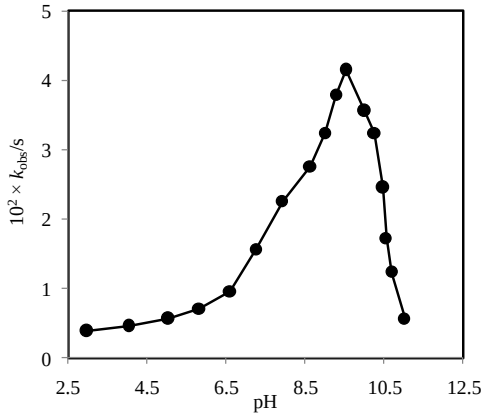

Preprints (www.preprints.org) | NOT PEER-REVIEWED | Posted: 22 January 2021 doi:10.20944/preprints202101.0434.v1

Figure 2. Observed rate constants (kobs) with solution pH within a range from 2.97 to 11.02 in I = 0.10 M ($NaNO_3$) at 25 ±1 °C. $[Ni^{2+}] = 1.00 \times 10^{-3}$ M; $[H_2TMPyP^{4+}] = 1.24 \times 10^{-5}$ M.

As described above, the speciation diagram exhibited the distribution of the Ni^{2+} species, $[Ni(H_2O)_{6-n}(OH)_n]^{2-n}$, with solution pH, accordingly, their kinetics were also different. According to equ (11), the rate constants such as k_1, k_2, k_3 and k_4 belong to hexaaquanickel(II), dihydroxonickel(II), trihydroxonickelate(II) and tetrahydroxonickelate(II) species, respectively. Thus, the individual rate constant was calculated by taking as a mean of the observed rate constants. The calculated observed rate constants are as follows: $k_1 = (0.62 \pm 0.22) \times 10^{-2}$; $k_2 = (3.60 \pm 0.40) \times 10^{-2}$; $k_3 = (2.09 \pm 0.52) \times 10^{-2}$, $k_4 = (0.53 \pm 0.04) \times 10^{-2}$ $M^{-1}s^{-1}$ at 25 ±1 °C in I = 0.10 M ($NaNO_3$) where $k_2 > k_3 > k_1 > k_4$. From this sequence, it is concluded that the aqua-monohydroxo Ni^{2+}, $[Ni(H_2O)_5(OH)]^+$, species exhibited the highest reactivity among the Ni^{2+} species in reacting with the $[H_2TMPyP]^{4+}$ where $k_2 = 3.60 \pm 0.40 \times 10^{-2}$ $M^{-1}s^{-1}$. It has been reported that monohydroxozinc(II), $[ZnOH]^+$, species exhibited the enhanced reactivity with non-N-substituted porphyrins where $k_{ZnOH^+} > k_{Zn^{2+}(aq)}$, that is comparable to that found in this study [18,55-57]. The enhanced rate constant has been ascribed to the formation of hydrogen bonding between the active oxygen atom of the hydroxo ligands and the pyrrolic hydrogen atom of the $[H_2TMPyP]^{4+}$. The $[ZnOH]^+$ species also exhibited enhanced reactivity towards N-p-nitrobenzyl-5,10,15,20-tetrakis(4-sulfonatophenyl)porphyrin [29]. It is noted that the formation of hydrogen bonding between the oxygen atom of the $[ZnOH]^+$ species and the pyrrolic hydrogen atom of the free base porphyrin is responsible for the enhanced reactivity. In the incorporation of Zn^{2+} ion into the $[H_2TMPyP]^{4+}$, the presence of hydroxo ligands of the Zn^{2+} species enhances the reactivity that obeys the following sequence: $k_{Zn(H2O)4(OH)2^0} > k_{Zn(H2O)3(OH)^-} > k_{Zn(H2O)5(OH)^+} > k_{Zn(H2O)6^{2+}}$ [25]. The monohydroxotrichloroaurate(III) species, $[AuCl_3(OH)]^-$, also showed enhanced reactivity towards the $[H_2TMPyP]^{4+}$ where $k_{AuCl3(OH)^-} > k_{AuCl4^-} > k_{AuCl2(OH)2^-} > k_{AuCl(OH)3^-}$ [24]. Schneider (1975) reported that monohydroxocopper(II), $[Cu(OH)]^+$, species exhibited much more reactivity towards the same free base porphyrin, $[H_2TMPyP]^{4+}$, compared to that of aquacopper(II), $Cu^{2+}(aq)$, species, i.e., $k_{Cu(OH)^+} >> k_{Cu^{2+}}$ [58]. The oxygen atom of the $[Cu(OH)]_+$ species forms H-bonding with the pyrrolic hydrogen atom of the porphyrin core. This is the reason for its substantial reactivity with the free base porphyrin. It is, therefore, concluded that the presence of the OH^- group of the aqua-monohydroxo, $[Ni(H_2O)_5(OH)]^+$, species make possible for the formation of hydrogen bonding with the pyrrolic hydrogen atom, thus the Ni^{2+} species can easily approach to the porphyrin's core. The formation of the hydrogen bonding and fast displacement of H_2O ligands from the Ni^{2+} species enhance the reactivity of the aqua-monohydroxo, $[Ni(H_2O)_5(OH)]^+$, species. However, the aqua Ni^{2+}, $[Ni(H_2O)_6]^{2+}$, species lack the hydroxo (OH^-) ligands, thus it might have less approaching ability to the porphyrin's core. This is the reason for less reactivity of the $Ni^{2+}(aq)$ species towards the $[H_2TMPyP]^{4+}$ ($k_1 = 0.62 \pm 0.22 \times 10^{-2}$ $M^{-1}s^{-1}$). The hexaaqua Ni^{2+} ion, $[Ni(H_2O)_6]^{2+}$, carries double positive charge that also decreases the reactivity of this species towards the tetracationic porphyrin, $[H_2TMPyP]^{4+}$. This is because of the development of Coulombic force of repulsion between the two positively charged species. It was expected to observe the highest reactivity for the aqua-dihydroxo, $[Ni(H_2O)_4(OH)_2]^0$, towards the $[H_2TMPyP]^{4+}$, however, $Ni(OH)_2^0$ begins to precipitate at pH ~8.20 for 10^{-3} M of Ni^{2+} solution using the log K^b_{S10} of -15.7 for the active $Ni(OH)_2^0$ [53]. In contrast, the aqua-dihydroxo species of Zn^{2+}, $[Zn(H_2O)_4(OH)_2]^0$, showed the highest reactivity among the $[Zn(H_2O)_{6-n}(OH)_n]^{n-2}$ species towards the free base porphyrin, $[H_2TMPyP]^{4+}$ [25]. Batinić-Haberle et al. (1999) used Marcus plot in order to determine the self-exchange rate constants for monohydroxoiron(III) porphyrins and aquamanganese(III) porphyrins, and they found that to be approximately 1 order of magnitude higher for the monohydroxoiron(III) porphyrins than those of aquamanganese(III) porphyrins [4].

However, the hydroxospecies having higher number of OH^- groups showed less reactivity towards the $[H_2TMPyP]^{4+}$ and the reactivity of the $[Ni(H_2O)_{6-n}(OH)_n]^{2-n}$ species

Preprints (www.preprints.org) | NOT PEER-REVIEWED | Posted: 22 January 2021 doi:10.20944/preprints202101.0434.v1

follows the decreasing sequence: $k_{Ni(H2O)5(OH)^+} > k_{Ni(H2O)4(OH)2^0} > k_{Ni(H2O)3(OH)3^-}$ (Fig. 3). Habib et al. (2004) reported that $AuCl_3(OH)^-$ exhibited the highest reactivity towards the free base porphyrin, $[H_2TMPyP]^{4+}$, among the $[AuCl_{4-n}(OH)_n]^-$ (n = 0,---,4) species according to the following sequence: $k_{AuCl3(OH)^-} > k_{AuCl2(OH)2^-} > k_{AuCl(OH)3^-}$ [24]. Paquette and Zador (1978) also reported that the reactivity of Zn^{2+} ion towards hematoporphyrin IX decreases with increasing number of the OH^- group coordinated to the Zn^{2+} ion and the reactivity order follows the sequence: $k_{Zn(OH)2^-} > k_{Zn(OH)3^-} > k_{Zn(OH)4^-}$ [55]. Cabbiness and Margerum (1969) reported that trihydroxocuprate(II), $[Cu(OH)_3]^-$, species shows higher reactivity towards the hematoporphyrin IX than the tetrahydroxocuprate(II), $[Cu(OH)_4]^{2-}$, i.e., $k_{Cu(OH)3^-} > k_{Cu(OH)4^{2-}}$ [30].

It is noteworthy to mention that the OH^- group coordinated to the metal ion plays crucial role for enhancing the reactivity of the metal species towards the $[H_2TMPyP]^{4+}$. This is because the oxygen atom of the aqua-monohydroxo, $[Ni(H_2O)_5(OH)]^+$, species forms hydrogen bonding with the pyrrolic hydrogen atom of the free base porphyrin, thus the aqua-monohydroxo species can easily approach to the porphyrin's core. The easy approach of the aqua-monohydroxonickel(II) species enhances its reactivity. On the other hand, the aqua Ni^{2+}, $[Ni(H_2O)_6]^{2+}$, species lacks of hydroxo ligand, so the aqua-species is incapable to form hydrogen bonding with the pyrrolic hydrogen atom. This is the reason for its less and/or least reactivity towards the $[H_2TMPyP]^{4+}$. However, the aqua-dihydroxo, $[Ni(H_2O)_4(OH)_2]^0$, species exhibited less reactivity with the free base porphyrin, $[H_2TMPyP]^{4+}$. This is because the aqua-dihydroxonickel(II) species takes part in hydrolysis reaction at solution pH 8.20 and then phases out from the aqueous system through precipitation reaction at higher pH, e.g., 9.50. The precipitation reaction causes lesser distribution of the dihydroxonickel(II) species compared to the aqua-monohydroxonickel(II) species at solution pH 9.50 (Fig. 1). The anionic trihydroxonickelate(II), $[Ni(H_2O)_3(OH)_3]^-$, species seems to be exhibited better reactivity towards the cationic porphyrin ($[H_2TMPyP]^{4+}$), however, the presence of the higher number of the hydroxo groups slows down its kinetics [24,25,30,55]. These results suggest that though the first OH- ligand is responsible for the formation of hydrogen bonding with the pyrrolic hydrogen atom, however, displacement of the remaining OH^- seems slow. It has been reported that the OH^- group is strongly coordinated to the metal ion having d^8 electronic configuration like Pt^{2+} ion [59]. The electronic configuration of Ni^{2+} is also d^8, so their chemical properties are supposed to be similar; hence the OH^- groups are also strongly coordinated with the Ni^{2+} ion. Bailey and Hambright (2003) reported that Cu^{2+} ion exhibited the highest reactivity among the other first transition metal ions, such as Zn^{2+}, Co^{2+} and Ni^{2+} towards the free base H_2-BrP(4)$^{4+}$ and tricationic H-BrP(4)$^{3+}$ porphyrins at 25 °C in I = 0.10 M ($NaNO_3$) and the reactivity order was found to be $Cu^{2+} > Zn^{2+} > Co^{2+} > Ni^{2+}$ [60]. It is expected that the reactivity of Ni^{2+} among the divalent metal ions towards the porphyrins would be less because of its d^8 electronic configuration. However, the presence of hydroxo-ligands with the Ni^{2+} species enhances its reactivity in incorporation with the free base porphyrin, $[H_2TMPyP]^{4+}$. Similar results have also been observed for Au^{3+} ion (d^8 electronic configuration) towards the $[H_2TMPyP]^{4+}$ [24].

3.3 Observed rate constants (k_{obs}) as a function of concentration of Ni^{2+}

Kinetics of the incorporation of Ni^{2+} ion into the $[H_2TMPyP]^{4+}$ with variation of the concentration of Ni^{2+} (I = 0.10 M, $NaNO_3$; pH 9.50) at 25 ±1 °C has also been studied in order to ascertain the formation rate constant for the metalation reaction. The observed rate constants (k_{obs}) with concentration of Ni^{2+} were obtained by plotting the $\ln(A_t\text{-}A_\alpha)$ vs time. The formation rate constant was obtained by plotting the observed rate constants (k_{obs}) with the concentration of Ni^{2+} as depicted in Figure 3. As seen from Fig. 3, the rate constant for the metalation reaction increases with increasing the concentration of Ni^{2+} and passes through the origin (r^2 = 0.999). This result suggests that the metalation reaction depends on concentrations of the both reacting species and follows the first order kinet-

Preprints (www.preprints.org) | NOT PEER-REVIEWED | Posted: 22 January 2021 doi:10.20944/preprints202101.0434.v1

ics. The formation rate constant (k_f) for the $[Ni(H_2O)_5(OH)]^+/[H_2TMPyP]^{4+}$ was found to be 3.99×10^{-2} $M^{-1}s^{-1}$ in I = 0.10 M ($NaNO_3$) at 25 ±1 ºC.

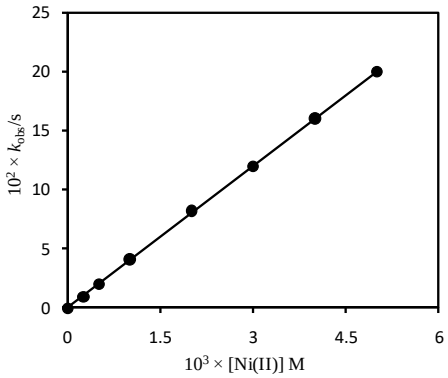

Figure 3. Dependence of the observed rate constants (k_{obs}) for the reaction of $[H_2TMPyP]^{4+}$ with on the concentration of Ni^{2+} in I = 0.10 M ($NaNO_3$) at 25 ±1 °C. $[H_2TMPyP^{4+}] = 1.24 \times 10^{-5}$ M; pH = 9.50.

3.4 Observed rate constants (k_{obs}) with ionic strength

The rate constants of a reaction for opposite charged reacting species decrease as the ionic strength increases while that increase for the same charged species [61]. Figure 4 shows the dependence the ionic strength on the rate constants for the reaction between the free base porphyrin, $[H_2TMPyP]^{4+}$, and Ni^{2+} species in I = 0 - 10.0×10^{-2} M ($NaNO_3$) at pH 9.50 where the experimental conditions were kept constant. The observed rate constants (k_{obs}) were obtained by plotting the $\ln(A_t\text{-}A_\alpha)$ vs time at different ionic strengths (Fig. 4). As seen from Figure 4, the observed rate constants (k_{obs}) exponentially decrease with the ionic strengths. These results suggest that the reacting compounds exist as oppositely charged species in solution, however, the speciation diagram is indicating the existence of the monopositive monohydroxo Ni^{2+}, $[Ni(H_2O)_5(OH)]^+$, species at solution pH 9.50. In our previous study, we also found the retardation of the kinetics between the dihydroxo Zn^{2+}, $[Zn(H_2O)_4(OH)_2]^0$, species and $[H_2TMPyP]^{4+}$ in the presence of $NaNO_3$ (I = 0.10 M) and the net charge of the porphyrin, $[H_2TMPyP]^{4+}$, was calculated to be +3.4 [Habib et al., 2020]. The rate constants for the incorporation of monohydroxotrichloroaurate(III), $[AuCl_3(OH)]^-$, into the $[H_2TMPyP]^{4+}$ also decrease exponentially with ionic strength and the calculated net charge of the free base porphyrin was found to be +3.4 by using the Fuoss equation [24]. However, in this study, we found a less decreasing tendency of the rate constants as the ionic strength increases. This may be due to the existence of monopositive monohydroxo Ni^{2+}, $[Ni(H_2O)_5(OH)]^+$, species that form adducts with the anionic/cationic species in the aqueous solution at pH 9.50 (Fig. 1 and Fig. 4). Hambright (2002) also reported that the rate constants for the reactions of the $[H_2TMPyP]^{4+}$ with Zn^{2+} species decrease as ionic strength increases, and the apparent net charge of the tetracationic porphyrin was found to be +1.4 by using the Bronsted-Bjerrum equation [6]. It seems that the direct reaction of the dipositive Ni^{2+} ion with the $[H_2TMPyP]^{4+}$ is strenuous, thus the presence of the nitrate ions causes to reduce the repulsive force between the $[Ni(H_2O)_5(OH)]^+$ species and the $[H_2TMPyP]^{4+}$ by interacting with the positively charged tetracationic porphyrin that facilitates the formation of aggregates of cation-anion with lower positive charge. Thus, it is assumed that the tetracationic free base porphyrin, $[H_2TMPyP]^{4+}$, carries relatively lower charge than the actual charge, +4.0 and probably both the monopositive monohydroxo, $[Ni(H_2O)_5(OH)]^+$, and neutral dihydroxo, $[Ni(H_2O)_4(OH)_2]^0$, species of Ni^{2+} ion took part in the reactions with the free base porphyrin, $[H_2TMPyP]^{4+}$, at pH 9.50 [6,24,25].

Preprints (www.preprints.org) | NOT PEER-REVIEWED | Posted: 22 January 2021 doi:10.20944/preprints202101.0434.v1

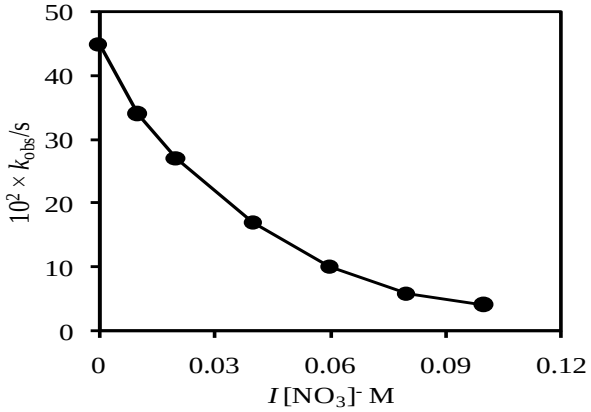

Figure 4. Observed rate constants, (k_{obs}), with ionic strengths ($NaNO_3$) at 25 ± 1 ºC. $[H_2TMPyP^{4+}]$ =1.24×10^{-5} M; $[Ni^{2+}]$ = 1.00 × 10^{-3} M; Solution pH: 9.50.

Figure 5 shows the Brønsted-Bjerrum plot for incorporation of Ni^{2+} ion into the tetracationic porphyrin, $[H_2TMPyP]^{4+}$. As seen from Fig. 5, regression coefficient (R^2), error bars and slope for the plot are 0.974, 1% and -3.60, respectively. It is expected that the intercept for the plot of logk_{obs} vs $\sqrt{I}$ should be zero, however, that is to be -0.273. This is because of the presence of inherent ions that cause intrinsic ionic strength. The slope for the plot is -3.60 that corresponds to Z_AZ_B. Thus, it is expected that the net charge of the tetracationic porphyrin would be +3.6. Nwaeme and Hambright (1984) studied the effects of ionic strength on the rate of the reactions for both the positive and negative porphyrins with divalent metal ions [62]. They reported that the rates of the reactions for positive porphyrins with positive divalent metal ions increase as increasing the ionic strength and that decrease for oppositely charged reacting species with the ionic strength. Williams et al. (1979) also reported the anionic effect on the reaction rate for tetracationic porphyrins in detergent solution [63].

According to the speciation diagram (Fig. 1), the predominant species of Ni^{2+} is monopositive monohydroxo, $[Ni(H_2O)_5(OH)]^+$, at solution pH 9.50. Thus, the rate of reaction of the tetracationic tetrakis(N-methylpyridium-4-yl)porphyrin, $[H_2TMPyP]^{4+}$, with the monopositive monohydroxonickel(II), $[Ni(H_2O)_5(OH)]^+$, species should be increased with increasing the ionic strength, however, that decreases as a function of ionic strength (Fig. 4). These results are suggesting the presence of anionic species of Ni^{2+} under the experimental conditions, however, speciation diagram (Fig. 1) shows the presence of monopositive monohydroxo, $[Ni(H_2O)_5(OH)]^+$, species at solution pH 9.50. The monopositive Ni^{2+} species, $[Ni(H_2O)_5(OH)]^+$, may associate with the inherent anion, thus forms negatively charged inner sphere reacting species in character such as ($[Ni(H_2O)_5(OH)]^+$-inherent anion)$^-$ [58,64]. The addition of nitrate ion reduces the positive charge of the cationic porphyrin at the transition state through formation of anion-cation-porphyrin adducts that causes the decreasing the reaction rates for negatively charged nickel species [18,58,65].

Preprints (www.preprints.org) | NOT PEER-REVIEWED | Posted: 22 January 2021 doi:10.20944/preprints202101.0434.v1

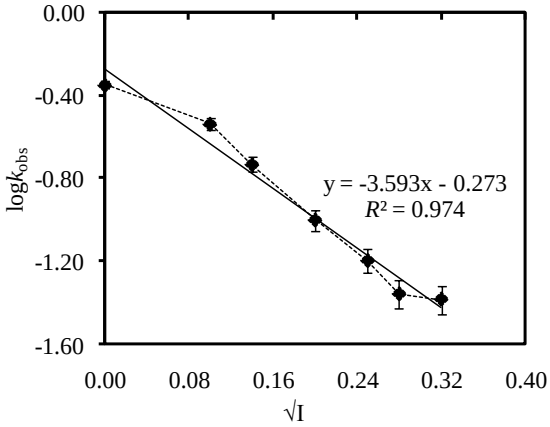

Figure 5. Brønsted-Bjerrum plot for nickel incorporation (1.00×10^{-3} M) into positive porphyrin, $[H_2TMPyP]^{4+}$, using Debye-Hückel Limiting (DHL) ionic strength function in $NaNO_3$ medium at 25 ± 1 ºC. Error bars represent a variation of 1%.

3.5 Interaction of $[Ni(II)TMPyP]^{4+}$ complex and $[H_2TMPyP]^{4+}$ with DNA

Figures 6a and b show the UV-vis spectral change of the $[Ni(II)TMPyP]^{4+}$ complex and the free base porphyrin, $[H_2TMPyP]^{4+}$, upon addition of DNA, respectively. As seen from Figure 6a, a small hypochromicity (~ 13%) at λ = 436 nm (λ_{max} of $[Ni(II)TMPyP]^{4+}$) and a very small Bathochromic shift ($\Delta\lambda$ = ~1 nm) were observed upon addition of DNA within a range from 0 to 7.96×10^{-6} M base pairs into the $[Ni(II)TMPyP]^{4+}$ solution. However, the free base porphyrin, $[H_2TMPyP]^{4+}$, displayed a substantial hypochromicity (~ 31%) at 422 nm (λ_{max} of $[H_2TMPyP]^{4+}$) and a wide Bathochromic shift ($\Delta\lambda$ = 17 nm) upon addition of the same DNA concentration (0 to 7.96×10^{-6} M base pairs) (Fig. 6b).

A fluorescence spectrophotometer was also used in order to investigate the interactions of the $[Ni(II)TMPyP]^{4+}$ and the $[H_2TMPyP]^{4+}$ with DNA (supplementary Fig. S-2). As seen from supplementary Figure S-2a, $[Ni(II)TMPyP]^{4+}$ complex exhibited a weak excitation fluorescence spectrum centered at 633 nm while the free base porphyrin, $[H_2TMPyP]^{4+}$, showed high excitation fluorescence spectrum centered at 660 nm with a hump at ~628 nm in the absence of DNA (supplementary Figure S-2b). The heavy atom effect by the nickel causes weak intensity for the $[Ni(II)TMPyP]^{4+}$ complex. In our previous study, we also found weak intensities from the Ru^{2+}-, Pd^{2+}-, Pt^{2+}- and $[Au(III)TMPyP]^{5+}$ porphyrins in aqueous solution because of the heavy atom effect [40,41].

The fluorescence intensity for the $[Ni(II)TMPyP]^{4+}$ complex is significantly decreased upon addition of a low concentration of DNA, and then increased with further addition of DNA (supplementary Figure S-2a). The porphyrin molecules aggregate on the negatively charged phosphate network of the DNA molecules through self-stacking in the presence of low concentration of DNA, however, de-aggregation occurs upon addition of additional DNA. This causes the increasing the fluorescence intensity of the metalloporphyrin [40,41].

Preprints (www.preprints.org) | NOT PEER-REVIEWED | Posted: 22 January 2021 doi:10.20944/preprints202101.0434.v1

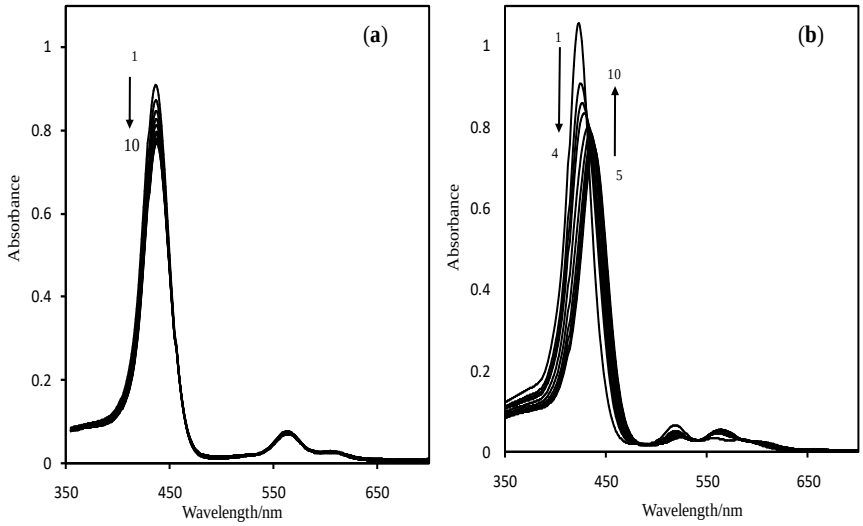

Figure 6. Changes in UV-vis spectra of (a) $[Ni(II)TMPyP]^{4+}$ and (b) $[H_2TMPyP]^{4+}$ in the presence of DNA of (1) 0, (2) 0.56 (3)1.12, (4) 3.33, (5) 4.43, (6) 5.52, (7) 6.06, (8) 6.88, (9) 7.42, (10) 7.96×10^{-6} M base pairs at pH 7.40 (HEPES). Total concentration of porphyrin is 1.14×10^{-5} M. Cell path length is 10 mm.

On the other hand, the intensity of the fluorescence centered at 660 nm did not change but the intensity of the hump appeared at ~628 nm is increased with a low concentration of DNA into the $[H_2TMPyP]^{4+}$ solution. The intensity of the hump increases with addition of DNA and the fluorescence spectrum is finally centered at 630 nm (supplementary Figure S-2b). These results suggested that the cationic free base porphyrin initially interacts with DNA via negatively charged phosphate network in the presence of a low concentration of DNA, and then de-stacking occurs upon further addition of DNA [40,41]. From the UV-vis and fluorescence spectral results, it is confirmed that both the metalloporphyrin, $[Ni(II)TMPyP]^{4+}$, and the free base porphyrin interact with DNA but their modes of interaction are different. As seen from Figure 6a, the hypochromicity and Bathochromic shift ($\Delta\lambda$) for the $[Ni(II)TMPyP]^{4+}$ are only ~ 13% (at λ_{max} 436 nm) and ~1 nm upon addition of high concentration of DNA, respectively. These results suggested that $[Ni(II)TMPyP]^{4+}$ interacts with DNA via outside binding with self-stacking [38-41,50,51]. However, the significant hypochromicity (~ 31% at 422 nm) and a wide Bathochromic shift ($\Delta\lambda$ = 17 nm) for the free base porphyrin upon addition of the same amount of DNA confirm its interaction with DNA through intercalation [38-41,50,51]. The presence of metal ion in the porphyrin core is responsible for carrying water molecules as axial ligands that make the bulkiness of the metalloporphyrin molecules. The large size of the metalloporphyrin molecules interact with DNA via outside binding rather than intercalation, however, the free base porphyrin interacts with DNA via intercalation because of its smaller size that facilitates easy excess into the DNA grooves. Metalloporphyrins that are outside binders have catalytic effects to cleave DNA [40,41,66], thus it is expected that the $[Ni(II)TMPyP]^{4+}$ complex can be used as a chemotherapeutic agent in the medical as well as in the biological fields.

4. Materials and Methods

4.1 Reagents and materials

The tetracationic free base porphyrin, 5,10,15,20-tetrakis(N-methylpyridinium-4-yl)porphyrin, $[H_2TMPyP]^{4+}$, was purchased as a tosylate from Dojindo Chemical Institute, Kumamoto, Japan. A 50 mL porphyrin solution was prepared by dissolving 68.18 mg of the free base porphyrin, $[H_2TMPyP]^{4+}$, in distilled water. A standard Cu^{2+} solution was used to standardize the porphyrin solution by using spectrophotometric titration (molar ratio method) [24,40,41]. Nickel solution

Preprints (www.preprints.org) | NOT PEER-REVIEWED | Posted: 22 January 2021 doi:10.20944/preprints202101.0434.v1

was prepared by dissolving requisite amount of $NiCl_2.6H_2O$ (Merck, Germany) in aqueous solution and the concentration was measured by using an atomic absorption spectrophotometer (Perkin Elmer, AAanalyst 200). Sodium nitrate, sodium hydroxide and hydrochloric acid were purchased from Merck, Germany. All the chemicals/reagents were used without further purification. Tetracation nickel(II) porphyrin, $[Ni(II)TMPyP]^{4+}$, was prepared and absorption spectra were recorded in water at pH 9.50 containing 0.10 M $NaNO_3$. Absorption maximum (λ_{max}) and molar extinction coefficient (ε) of the prepared $[Ni(II)TMPyP]^{4+}$ complex were 436 nm and 114×10^3 $M^{-1}cm^{-1}$, respectively (Fig. 1) [67].

A stock solution of salmon fish sperm DNA, purchased from Sigma-Aldrich, was prepared by dissolving in distilled water and the concentration in base pairs was determined by knowing the absorbance at λ_{max} = 260 nm and using the molar extinction coefficient, ε_{260} =1.32×10^4 $M^{-1}cm^{-1}$ [40,41]. Stock solution of the DNA was kept in a refrigerator at -4 ºC. The frozen DNA solution was incubated in a water bath at 37 ºC for an hr and diluted as required before the experiment. Acetate/sodium acetate and 2-[4-(2-hydroxyethyl)-1-piperazinyl]ethanesulfonic acid (HEPES, Sigma-Aldrich) buffer solution were prepared in 100 mL distilled water as stock solutions and used with required dilution throughout the experiments. pH of the HEPES solution (0.10 M) was adjusted to 7.40 upon addition of either NaOH or HCl. In this work, distilled water was used to perform all the experiments.

4.2 Speciation of Ni(II) complexes

Solutions of 5.00×10^{-3} M $NiCl_2$ with changing solution pH from 2.97 to 11.40, were prepared in 50 mL volumetric flasks separately. The requisite volume of sodium nitrate was added to each solution in order to maintain ionic strength (I = 0.10 M). Solution pH was adjusted by addition of either HCl or NaOH in acetate buffer ([Acetate] = 0.02 M). The UV-Vis spectra of the Ni^{2+} species were recorded by using a double beam UV-Vis spectrophotometer (SHIMADZU, Model UV-1800) within a range from 350 to 500 nm. A number of Ni^{2+} solutions (5.00×10^{-3} M) with different concentration of acetate ion ranging from 0 to 1.00×10^{-2} M was prepared under the same experimental conditions to investigate the interaction between Ni^{2+} and acetate ions and found no formation of Ni(II)-acetate complex. A pH meter (HANNA HI 2211) was used to measure the solution pH.

4.3 Kinetics of formation of $[Ni(II)TMPyP]^{4+}$ complex

Pseudo-first order condition was kept constant throughout the experiment in order to explore the kinetics of the reactions between tetracationic free base porphyrin and Ni^{2+} species in I = 0.10 M ($NaNO_3$) at 25 ±1 ºC where the pH of the solutions were varied from 2.97 to 11.05. Concentration of Ni^{2+} was varied from 0.50×10^{-3} to 5.00×10^{-3} M while that for the porphyrin, $[H_2TMPyP]^{4+}$, was kept constant at 1.24×10^{-5} M. The metalloporphyrin was prepared by mixing the porphyrin solution with the Ni^{2+} solution in a 1-cm cell compartment and pre-equilibrated at 25 ±1 ºC. The change in the absorbance was monitored as a function of time at 422 nm (λ_{max} of $[H_2TMPyP]^{4+}$) by using a UV-Vis spectrophotometer (SHIMADZU, Model UV-1800). Formation of the $[Ni(II)TMPyP]^{4+}$ complex was monitored by observing isosbestic points at 431, 490 and 546 nm in the visible region as the porphyrin reacted with the Ni^{2+} species. Appearing the isosbestic points is confirming the free base porphyrin and Ni(II)porphyrin complex are only the absorbing species. Figure 7 shows such a spectral pattern of the formation of the $[Ni(II)TMPyP]^{4+}$ complex with time. To obtain the observed rate constants (k_{obs}), values of $\ln(A_t\text{-}A_\alpha)$ were plotted with time and found linearity over two half-lives. Rate constants for the reactions between the free base porphyrin and Ni^{2+} species were determined by varying solution pH, nickel concentrations and ionic strengths. The duplicate runs under the same conditions agreed within 5% error. A pH meter (HANNA HI 2211) was used to measure the solutions pH.

Preprints (www.preprints.org) | NOT PEER-REVIEWED | Posted: 22 January 2021 doi:10.20944/preprints202101.0434.v1

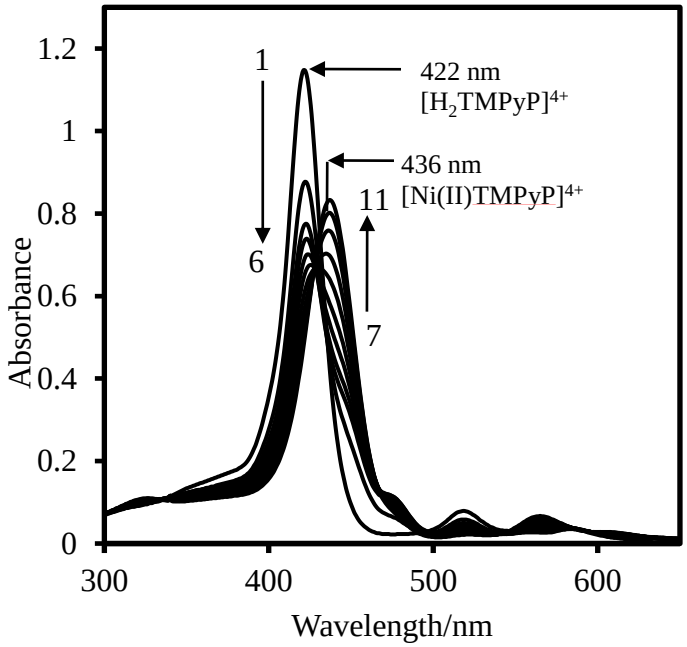

Figure 7. Absorption spectra of $[Ni(II)TMPyP]^{4+}$ complex with time at solution pH = 9.50 (25 °C) in I = 0.10 M ($NaNO_3$). $[Ni^{2+}]$ = 1.00 × 10^{-3} M; $[H_2TMPyP]^{4+}$ = 1.24 × 10^{-5} M. Progress of the formation of the $[Ni(II)TMPyP]^{4+}$ complex was monitored by changing the absorbance of $[H_2TMPyP]^{4+}$ at λ_{max} = 422 nm with time. The formation time are as follows: (1): 0; (2): 5; (3) 10; (4): 20; (5): 30; (6): 50; (7): 70; (8): 100; (9): 140; (10): 200; (11): 260 min, respectively.

2.4 Interaction of $[Ni(II)TMPyP]^{4+}$ complex with DNA

The UV-Vis spectra of the free base porphyrin and $[Ni(II)TMPyP]^{4+}$ complex upon addition of DNA were recorded by using a double-beam UV-Vis spectrophotometer (UV-1800, Shimadzu, Japan). A fluorescence spectrophotometer (F-7000, Hitachi, Japan) was used to record the luminescence spectra for the free base porphyrin and the Ni(II)porphyrin in the presence of DNA. The fluorescence emission wavelength was scanned from 550 to 800 nm by setting the excitation wavelength at 446 and 431 nm for the $[Ni(II)TMPyP]^{4+}$ and $[H_2TMPyP]^{4+}$, respectively. This is because the isosbestic points for the binary system of $[Ni(II)TMPyP]^{4+}$-DNA and $[H_2TMPyP]^{4+}$-DNA were observed at 446 and 431 nm, respectively. Under the present experimental conditions, for 1.14 × 10^{-5} M of $[Ni(II)TMPyP]^{4+}$ and $[H_2TMPyP]^{4+}$, the absorbance and luminescence spectra of the porphyrin solutions were not affected by the species adsorbed on the surface of the cell wall. These were confirmed by recording a UV-vis spectrum of ethanol-water after discarding the analyte solution and found no peaks from the ethanol-water. All the experiments were carried out under room light. HEPES solution of 0.02 M (pH 7.40) was used throughout the experiment. A pH meter (HANNA HI 2211) was used to measure the solution pH.

5. Conclusion

In this work, kinetics and mechanism of formation of $[Ni(II)TMPyP]^{4+}$ have been studied at 25 ±1 ºC in I = 0.10 M ($NaNO_3$) within a pH range from 2.97 to 11.40 in aqueous medium. Speciation of Ni^{2+} ions in aqueous medium has also been done in 0.10 M $NaNO_3$ in order to provide the distribution of the Ni^{2+} species as a function of solution pH for the kinetic study. The experimental data have been compared with the speciation diagram generated from the values of hydrolysis constants of Ni^{2+} ion. The speciation

data exhibited the stepwise formation of $[Ni(H_2O)_{6-n}(OH)_n]^{2-n}$ species as a function of solution pH. Kinetic studies showed that aqua-monohydroxo, $[Ni(H_2O)_5(OH)]^+$, species showed the highest reactivity towards the free base porphyrin, $[H_2TMPyP]^{4+}$. The formation of hydrogen bonding between the oxygen atom of the hydroxo-ligand of the $[Ni(H_2O)_5(OH)]^+$ species and the pyrrolic hydrogen atom of the $[H_2TMPyP]^{4+}$ enhances the reactivity of the aqu-monohydroxonickel(II) species. Ionic strength effect on the reaction rate is suggested that the net charge of the tetracationic is supposed to be +3.6 on the basis of Brønsted-Bjerrum equation. It has been expected that the rate of incorporation of the $[Ni(H_2O)_5(OH)]^+$ species into the $[H_2TMPyP]^{4+}$ would be slow but showed fast. From the UV-Vis and fluorescence spectroscopic results, it is concluded that the $[Ni(II)TMPyP]^{4+}$ complex and $[H_2TMPyP]^{4+}$ interact with DNA where UV-Vis data revealed that the metallo-complex follows outside binding with self-stacking with DNA while the free base porphyrin shows intercalation. Metalloporphyrins that are outside binders have catalytic effects to cleave DNA, thus the $[Ni(II)TMPyP]^{4+}$ complex could be used as a chemotherapeutic agent in the medical as well as in the biological fields. An investigation of the application of the $[Ni(II)TMPyP]^{4+}$ complex with other metalloporphyrins, for example, Zn^{2+}-, Ru^{2+}-, Pt^{2+}-, $[Au(III)TMPyP]^{5+}$ as anti-COVID-19 agents is now in progress under international collaboration.

Additional information

Supplementary information

Acknowledgements

The authors acknowledge to the Ministry of Science and Technology, People's Republic of Bangladesh for financial support to carry out this work under the project "Photoelectrochemical splitting of water into hydrogen using solar light".

Competing interests

The authors declare no competing financial/commercial interest.

Authors contribution statement

Ahsan Habib: Conceptualization, Supervision, Writing original draft-review, Final review & editing, Funding acquisition, Salma Serniabad: Formal analysis, Data curation, Experimental results analysis; Mohammad Shamim Khan: Formal analysis, Data curation, Experimental results analysis; Rokayea Islam: Formal analysis, Data curation, Experimental results analysis; Mrittika Chakraborty: Formal analysis, Data curation, Experimental results analysis; Aklima Nargis: Investigation, Data curation: Md Emran Quayum: Conceptualization, Supervision, Funding acquisition, Md Ashraful Alam: Conceptualization, Supervision, Valentina Rapozzi: Conceptualization, Final review & editing, Masaaki Tabata: Conceptualization, Final review & editing. All the authors have read and agreed to the published version of the manuscript.

References

1. Pasternack, R.F.; Skowronek, W.R. Jr. Catalysis of the disproportionation of superoxide by metalloporphyrins. *J. Inorg. Biochem*. **1979**, 11(3), 261-267.
2. Marzilli, L. G. Medical Aspects of DNA-Porphyrin Interaction. *New J. Chem*. **1990**, 14, 409-420.
3. DeCamp, D.L.; Babé, L.M.; Salto, R.; Lucich, J.L.; Koo, M.S.; Kahl, S.B.; Craik, C.S. Specific inhibition of HIV-1 protease by boronated porphyrins. *J. Med. Chem*. **1992**, 35, 3426-3428.
4. Batinić-Haberle, I.; Spasojević, I.; Hambright, P.; Benov, L.; Crumbliss, A.L.; Fridovich, I. Relationship among Redox Potentials, Proton Dissociation Constants of Pyrrolic Nitrogens, and in Vivo and in Vitro Superoxide Dismutating Activities of Manganese(III) and Iron(III) Water-Soluble Porphyrins. *Inorg. Chem*. **1999**, 38, 4011-4022.
5. Sasaki, K.; Yumita, N.; Nishigaki R., Sakata, I.; Nakajima, S.; Umemura, S.I. Pharmacokinetic study of a gallium-porphyrin photo- and sono-sensitizer, ATX-70, in tumor-bearing mice. *Jpn. J. Cancer Res*. **2001**, 92, 989-995.
6. Hambright, P. (2002). In: The Porphyrin Handbook, Kadish, K.M., Smith, K.M. and Guilard, R. (Eds.), 163, Academic Press.

7. Lin, L.; Hu, J. Inhibition of hepadnavirus reverse transcriptase-epsilon RNA interaction by porphyrin compounds. *J. Virol*. **2008**, 82, 2305-2312.
8. Batinic-Haberle, I.; Reboucas, J.; Spasojevic, I. Superoxide dismutase mimics: chemistry, pharmacology and therapeutic potential. *Antioxid. Redox Signal*. **2010**, 13, 877-918.
9. Cheng, Y.; Tsou, L.K.; Cai, J.; Aya, T;, Dutschman, G.E.; Gullen, E.A.; Grill, S.P.; Chen, A.P.; Lindenbach, B.D.; Hamilton, A.D.; Cheng, Y.C. A novel class of meso-tetrakis-porphyrin derivatives exhibits potent activities against hepatitis C virus genotype 1b replicons in vitro. *Antimicrob. Agents Chemother*. **2010**, 54, 197-206.
10. Guo, H.; Pan, X.; Mao, R.; Zhang, X.; Wang, L.; Lu, X.; Chang, J.; Guo, J.-T.; Passic, S.; Krebs, F.C.; Wigdahl, B.; Warren, T.K.; Retterer, C.J.; Bavari, S.; Xu, X.; Cuconati, A.; Block, T.M. Alkylated Porphyrins Have Broad Antiviral Activity against Hepadnaviruses, Flaviviruses, Filoviruses, and Arenaviruse. *Antimicrob. Agents Chemother*. **2011**, 2, 478-486.
11. Rapozzi, V.; Zorzet, S.; Zacchigna, M.; Pietra, E.D.; Cogoi, S.; Xodo, L.E. Anticancer activity of cationic porphyrins in melanoma tumour-bearing mice and mechanistic in vitro studies. *Molecular Cancer* **2014**, 13, 75.
12. Tovmasyan, A.; Sampaio, R.S.; Boss, M.K.; Bueno-Janice, J.C.; Bader, B.H.; Thomas, M.; Reboucas, J.S.; Orr, M.; Chandler, J.D.; Go, Y.M.; Jones, D.P.; Venkatraman, T.N.; Haberle, S.; Kyui, N.; Lascola, C.D.; Dewhirst, M.W.; Spasojevic, I.; Benov, L.; Batinic-Haberle, I. Anticancer therapeutic potential of Mn porphyrin/.ascorbate system. *Free Radic. Biol. Med*. **2015**, 89, 1231-1247.
13. Varchi, G.; Foglietta, F.; Canaparo, R.; Ballestri, M.; Arena, F.; Sotgiu, G.; Fanti, S. Engineered porphyrin loaded core-shell nanoparticles for selective sonodynamic anticancer treatment. *Nanomedicine* **2015**, 10, 3483-3494.
14. Su, S.; Ding, Y.; Li, Y.; Wu, Y.; Nie, G. Integration of photothermal therapy and synergistic chemotherapy by a porphyrin self-assembled micelle confers chemosensitivity in triple-negative breast cancer. *Biomater*. **2016**, 80, 169-178. DOI: 10.1016/j.biomaterials.2015.11.058
15. Malatesti, N.; Munitic, I.; Jurak, I. Porphyrin-based cationic amphiphilic photosensitisers as potential anticancer, antimicrobial and immunosuppressive agents. *Biophys. Rev*. **2017**, 9, 149-168.
16. Batinic-Haberle, I.; Tovmasyan, A.; Spasojevic, I. Mn Porphyrin-Based Redox-Active Drugs: Differential Effects as Cancer Therapeutics and Protectors of Normal Tissue Against Oxidative Injury. *Antioxid Redox Signal*. **2018**, 29(16), 1691-1724.
17. Tebo, A.; Herrero, C.; Aukauloo, A. In *Porphyrins and Metalloporphrins as Components in Artificial Photosynthesis Research*, Handbook of Porphyrin Science; Kadish, K.M., Smith, K.M. and Guilard, R.; Eds.; World Scientific, 2014; pp. 195-237
18. Hambright, P; Chock, P.B. Metal-porphyrin interactions. III. Dissociative-interchange mechanism for metal ion incorporation into porphyrin molecules. *J. Am. Chem. Soc*. **1974**, 96, 3123-3131.
19. Hambright, P. In *Porphyrins and Metalloporphyrins*, Smith, K.M.; Eds., Elsevier, 1975; pp.233-278.
20. Tanaka, M. Kinetics of metalloporphyrin formation with particular reference to the metal ion assisted mechanism. *Pure Appl. Chem*. **1983**, 55, 151-158.
21. Lavallee, D.K. Kinetics and mechanisms of metalloporphyrin reactions. *Coord. Chem. Rev*. **1985**, 61, 55-96.
22. Funahashi, S.; Ito, Y.; Kakito, H.; Inamo, M.; Hamada, Y.; Tanaka, M. Metal ion incorporation into n-methyl-5,10,15,20-tetrakis (4-sulfonatophenyl) porphine and its differential rates as applied to the kinetic determination of copper(II) and zinc(II) in serum. *Microchim. Acta* **1986**, 88, 33-47.
23. Tabata, M.; Tanaka, M. Porphyrins as reagents for trace-metal analysis. *TrAC Trends Anal. Chem*. **1991**, 10, 128-133.
24. Habib, A.; Tabata, M.; Wu, Y. Kinetics and mechanism of gold(III) incorporation into tetrakis(1-methylpyridium-4-yl)porphyrin in aqueous solution. *J. Porphyrins Phthalocyanines* **2004**, 8, 1269-1275.
25. Habib, A.; Islam, R.; Chakraborty, M.; Serniabad, S.; Khan, M.S.; Qais, D.S.; Quayum, M.E.; Alam, M.A.; Ismail, I.M.I.; Tabata, M. Kinetics and mechanism of incorporation of zinc(II) into tetrakis(1-methylpyridium-4-yl)porphyrin in aqueous solution. *Arab. J. Chem*. **2020**, 13, 6552-6558.
26. Margerum, D.W; and Cayley, G.R. In *Coordination Chemistry*, Martell, A.E.; Ed., American Chemical Society, USA; 1978; pp.1-194.
27. Shamim, A.; Hambright, P. Exchange reactions of transition metal ions and labile cadmium porphyrins. *J. Inorg. Nucl. Chem*. **1980**, 42, 1645-1647.
28. Tabata, M.; Tanaka, M. Kinetics and mechanism of cadmium(II) ion assisted incorporation of manganese(II) into 5,10,15,20tetrakis(4-sulphonatophenyl)porphyrinate(4-). *J. Chem. Soc., Dalton Transac*. **1983**, 1955-1959.
29. Tabata, M.; Ishimi, H. Kinetics and mechanism for the formation and dissociation reactions of 21-(4-nitrobenzyl)-5,10,15,20-tetrakis(4-sulfonatophenyl)-23H-porphyrinatozinc(II) and -cadmium(II). *Bull. Chem. Soc. Jpn*. **1997**, 70, 1353-1359.
30. Cabbiness, D.K.; Margerum, D. Macrocyclic effect on the stability of copper(II) tetramine complexes. *J. Am. Chem. Soc*. **1969**, 91, 6540-6541.
31. Lavellee, D.K. In *The Chemistry and Biochemistry of N-Substututed Porphyrins*, VCH Publishers, Germany; 1987; pp. 1-313.
32. Bain-Ackerman, M.J.; Lavallee, D.K. Kinetics of metal-ion complexation with N-methyltetraphenylporphyrin. Evidence concerning a general mechanism of porphyrin metalation. *Inorg. Chem*. **1979**, 18, 3358-3364.
33. Turay, J.; Hambright, P. Activation parameters and a mechanism for metal-porphyrin formation reactions. *Inorg. Chem*. **1980**, 19, 562-564.
34. Sato, T.; Ebisawa, K.; Sue, K.; Ito, S.; Saito, T.; Itoh, N. The Kinetics of the incorporation of metals into tetraphenylporphyrin with metal salts in high-temperature water. *Indust. Eng. Chem. Res*. **2012**, 51, 13908-13914.

35. Peters, M.K.; Herges, R. Insertion of Ni(I) into porphyrins at room temperature: preparation of Ni(II)porphyrins, and Ni(II)chlorins and observation of hydroporphyrin intermediates. *Inorg. Chem*. **2018**, 57, 3177-3182.
36. Tan, X.L.; Hu, J.; Montavon, G.; Wang, X.K. Sorption Speciation of Nickel(II) onto Ca-Montmorillonite: Batch, EXAFS Techniques and Modeling. *Dalton Transac*. **2011**, 41.
37. Tian, Y.; Etschmann, B.; Liu, W.; Borg, S.; Mei, Y.; Testemale, D.; O'Neill, B.; Rae, N.; Sherman, D.M.; Ngothai, Y.; Johannessen, B.; Glover, C.; Brugger, C. Speciation of nickel(II) chloride complexes in hydrothermal fluids: In situ XAS study. **Chem. Geolog**. *2012*, 334, 345-363.
38. Carvlin, M.J.; Fiel, R.J. Intercalative and nonintercalative binding of large cationic porphyrin ligands to calf thymus DNA. *Nucl. Acids Res*. **1983**, 11, 6121-6139.
39. Guliaev, A.B.; Leontis, N.B. Cationic 5,10,15,20-tetrakis(N-methylpyridinium-4-yl)porphyrin fully intercalates at 5'-CG-3' steps of duplex DNA in solution. *Biochem*. **1999**, 38, 15425-15437.
40. Nyarko, E.; Hanada, N.; Habib, A.; Tabata, M. Fluorescence and phosphorescence spectra of Au(III), Pt(II) and Pd(II) porphyrins with DNA at room temperature. *Inorg. Chim. Acta* **2004**. 357, 739-745.
41. Habib, M.A.; Sarker, A.K.; Tabata, M. Interactions of DNA with H2TMPyP4+and Ru(II)TMPyP4+: Probable Lead Compounds for African Sleeping Sickness. *Bangladesh Pharma. J*. **2014**, 17, 79-85.
42. Wang, M.; Mao, Z.; Kang, T.-S.; Wong, C.-Y.; Mergny, J.-L.; Leung, C.-H.; Ma, D.-L. Conjugating a groove-binding motif to an Ir(iii) complex for the enhancement of G-quadruplex probe behavior. *Chem. Sci*. **2016**, 7, 2516-2523.
43. Chao, X.-J.; Tang, M.; Huang, R.; Huang, C.-H.; Shao, J.; Yan, Z.-Y.; Zhu, B.-Z. Targeted live-cell nuclear delivery of the DNA 'light-switching' Ru(II) complex via ion-pairing with chlorophenolate counter-anions: the critical role of binding stability and lipophilicity of the ion-pairing complexes. *Nucl. Acids Res*. **2019**, 47, 10520-10528.
44. Williamson, A.; Leiros, H.-K.S. Structural intermediates of a DNA-ligase complex illuminate the role of the catalytic metal ion and mechanism of phosphodiester bond formation. *Nucl. Acids Res*. **2019**, 47, 7147-7162.
45. Spence, P.; Fielden, J.; Waller, Z.A.E. Beyond solvent exclusion: i-Motif detecting capability and an alternative DNA light-switching mechanism in a ruthenium(II) polypyridyl complex. *J. Am. Chem. Soc*. **2020**, 142, 13856-13866.
46. Ptaszynska, A.A.; Trytek, M.; Borsuk, G.; Buczek, K.; Rybicka-Jasin´ska, K.; Gryko, D. Porphyrins inactivate Nosema spp. *Microsporidia. Sci. Rep*. **2018**, 8, 5523.
47. Fazaeli, Y., Jalilian, A.R., Amini, M.M., Aboudzadeh, M., Feizi, S., Rahiminezhad, A. and Yousefi, K. (2013a). Preparation, nano purification, quality control and labeling optimization of [64Cu]-5,10,15,20-tetrakis (penta fluoro phenyl) porphyrin complex as a possible imaging agent. *J. Radioanal. Nucl. Chem*. **2013a**, 295, 255-263.
48. Fazaeli, Y.; Jalilian, A.R.; Feizi, S.; Shadanpour, N. Development of a radiothallium(III) labeld porphyrin complex as a potential imaging agent. *Radiochim. Acta* **2013b**, 101, 795-800.
49. Vahidfar, N.; Jalilian, A.R. An Overview of Labeled Porphyrin Molecules in Medical Imaging. *Recent Patents Topics Imag*. **2015**, 5, 3-12.
50. Dougherty, G. Intercalation of tetracationic metalloporphyrins and related compounds into DNA. *J. Inorg. Biochem*. **1988**, 34, 95-103.
51. Fiel, R.J. Porphyrin-nucleic acid interactions: a review. *J. Biomol. Struc. Dyn*. **1989**, 6, 1259-1274.
52. Liu, W.; Li, H. COVID-19 Disease: ORF8 and Surface Glycoprotein Inhibit Heme Metabolism by Binding to Porphyrin. *ChemRxiv*. **2020**. https://doi.org/10.26434/chemrxiv.11938173.v2.
53. Baes, C.F.; Mesmer, R.E. In *The Hydrolysis of Cations*. Wiley, New York, USA; 1976; p. 246.
54. Atkins, P.; Overton, T.; Rourke, J.; Weller, M.; Armstrong, F. In *Shriver & Atkins' Inorganic Chemistry*, 5th edition, Oxford University Press, UK; 2014.
55. Paquette, G.; Zador, M. Kinetics of interaction of Zn(II) with hematoporphyrin IX in basic aqueous solution. *Inorg. Chim. Acta* **1978**, 26, L23-L24.
56. Thompson, A.N.; Krishnamurthy, M. Peripheral charge effects on the kinetics of Zn(II)-porphyrin system. *J. Inorg. Nucl. Chem*. **1979**, 41, 1251-1255.
57. Sutter, T.P.G.; Hambright, P. The effects of peripheral substituents on the kinetics of zinc ion incorporation and acid catalyzed removal from water soluble sulfonated porphyrins. *J. Coord. Chem*. **1993**, 30, 317-326.
58. Schneider, W. Kinetics and mechanism of metalloporphyrin formation. In *Biochemistry. Structure and Bonding*, 23. Springer, Berlin, Germany, 1975; Heidelberg.
59. Pearson, R.G. Hard and soft acids and bases. *J. Am. Chem. Soc*.**1963**, 85, 3533-3539.
60. Bailey, S.L.; Hambright, P. Kinetics of the reactions of divalent copper, zinc, cobalt, and nickel with a deformed water soluble centrally monoprotic porphyrin. *Inorg. Chim. Acta* **2003**, 344, 43-48.
61. Castaneda-Agullo, M.; Del Castillo, L.M.; Whitaker, J.R.; Tappel, A.L. Effect of ionic strength on the kinetics of trypsin and alpha chymotrypsin. *J. Gen. Physiol*. **1961**, 44, 1103-20.
62. Nwaeme, J.; Hambright, P. Magnitudes of ionic strength effects in porphyrin metalation and acid solvolysis reactions. *Inorg. Chem*. **1984**, 23 (13), 1990-1992.
63. Williams, G.; Williams, R.F.X.; Lewis, A.; Hambright, P. J. Synthesis, characterization and copper incorporation into 5-(4-pyridyl)-10,15,20-triphenylporphyrin. *Inorg. Nucl. Chem*. **1979**, 41, 41-44.
64. Longo, F. In *The Porphyrins*, Dolphin, D.; Ed.; Academic Press, New York, USA, 1978; 5, Ch. 10.

 doi:10.20944/preprints202101.0434.v1

65. Rau, W.G.; Longo, F.R. Study of the aqueous equilibrium system involving meso-tetrapyridylporphine, alkali metal ions, and hydrogen ions. *Inorg. Chem*. **1977**, 16, 6, 1372-1376.
66. Tabata, M.; Nakajima, K.; Nyarko, E. Metalloporphyrin mediated DNA cleavage by a low concentration of HaeIII restriction enzyme. *J. Inorg. Biochem*. **2000**, 78, 383-389.
67. Hambright, P. In *Chemistry of Water Soluble Porphyins*, Kadish, K.M., Smith, K.M.; Guilard, R., Eds.; Academic Press,New York, USA, 2020; p.199.